Optical spectroscopy of $Yb_2Ti_2O_7$ and $Y_2Ti_2O_7:Yb^{3+}$ and crystal-field parameters in rare-earth titanate pyrochlores

B. Z. Malkin and A. R. Zakirov
Physics Department, Kazan State University, Kremlevskaya 18, 420008 Kazan, Russian Federation

M. N. Popova, S. A. Klimin, and E. P. Chukalina
Institute of Spectroscopy, Russian Academy of Sciences, 142190 Troitsk, Moscow Region, Russian Federation

E. Antic-Fidancev, Ph. Goldner, and P. Aschehoug
Laboratoire de Chimie Appliquee de l'État Solide, CNRS UMR 7574, ENSCP, F-75231 Paris Cedex 05, France

G. Dhalenne
Laboratoire de Physico-Chimie de l'État Solide, Université Paris-Sud, F-91405 Orsay, France
(Received 17 February 2004; published 27 August 2004)

Optical absorption spectra of the $Yb_2Ti_2O_7$ single crystals and luminescence spectra of the $Y_2Ti_2O_7:Yb$ (1%) polycrystalline samples were registered at temperatures 4.2–300 K. These spectra and earlier published data on magnetic properties of Yb^{3+} ions and on the temperature dependence of the electric field gradient at Yb nuclei in $Yb_2Ti_2O_7$ were used to analyze the crystal-field parameters in rare-earth titanates with the pyrochlore structure. The self-consistent sets of crystal-field parameters for rare-earth ions in the 16*d* sites with the D_{3d} symmetry that describe satisfactory all known single-ion magnetic properties and low-energy excitations in $R_2Ti_2O_7$ crystals (R=Tb, Ho, Er, Tm, Yb) are presented.

DOI: 10.1103/PhysRevB.70.075112 PACS number(s): 78.30.−j, 78.55.Hx, 78.20.Bh

I. INTRODUCTION

The insulating pyrochlore rare-earth (R) oxides described by the general formula $R_2A_2O_7$ (A=Ti, Sn, Zr, Hf) have the face-centered cubic crystal structure with the space group $Fd\bar{3}m$, in which R and nonmagnetic transition-metal A^{4+} ions are situated at the sublattices of corner-sharing tetrahedra and occupy the sites 16*d* and 16*c*, respectively, with the D_{3d} symmetry.[1–4] These compounds have unusual thermodynamic and dynamic magnetic properties at low temperatures, which has drawn much attention of the physicists (see Refs. 5–7, and references therein). There are four different but crystallographically equivalent trigonal symmetry axes corresponding to the tetrahedron four-corner sites. Magnetic moments of R^{3+} ions (except Gd^{3+}) in the trigonal crystal field are strongly anisotropic. In particular, the non-Kramers Tb^{3+} and Ho^{3+} ions, and the Kramers Dy^{3+} ions situated at the tetrahedra corners have in their ground state axial magnetic moments pointing into or out of the center of each tetrahedron. In the case of the ferromagnetic isotropic exchange interactions between these Ising ions, no single spin configuration realizes a local energy minimum for all pairs of spins, the magnetic moments are "frustrated." This means that spin configurations of the ground state on a tetrahedron formed by "two-out" and "two-in" magnetic moments are sixfold degenerate. The ground state of the spin system, corresponding to these spin-ice structures (similar to proton configurations in the ordinary hexagonal ice), is macroscopically degenerate. The long-range magnetic order is absent in $Tb_2Ti_2O_7$, $Ho_2Ti_2O_7$, $Dy_2Ti_2O_7$ down to 15 mK,[8–11] 46 mK,[12,13] and 60 mK,[14] respectively. At low temperatures, the spin freezing was observed with specific spin correlations and a local short-range order. In particular, the spin-ice structure was found in $Ho_2Ti_2O_7$ (Refs. 15,16) and $Dy_2Ti_2O_7$,[17] the spin-liquid behavior was observed in $Tb_2Ti_2O_7$.[18] However, in contrast to crystals containing the Ising-type ions ($g_\perp=0$), the pyrochlore erbium titanate where magnetic moments of Er^{3+} ions are confined to the planes (111) ($g_\perp > g_\parallel$) is the XY antiferromagnet below $T_N=1.17$ K.[19]

As the Ho^{3+}, Dy^{3+}, and Tb^{3+} ions in the pyrochlore oxides have large magnetic moments close to their maximum values,[6,18] the magnetic dipole-dipole interaction plays a dominant role in the cooperative behavior of these magnetic ions. The long-range nature of this interaction opens a possibility of magnetic ordering at low temperatures even if a slightly weaker superexchange interaction between the nearest neighbors exists. However, the ordered states predicted by the corresponding dipolar spin-ice model[20] were not revealed. Experimental observation of a magnetically ordered phase depends on the thermalization rate of the spin system at the actual time scale and its dynamical properties. The geometric frustration of interion interactions causes peculiarities of the cooperative magnetic behavior of the spin system while the single-ion magnetic properties are predetermined by the crystal field (CF) that splits the ground multiplet of a R^{3+} ion. In particular, interion distances in the pyrochlore stannate are larger by about 4% than in the titanate of the same rare-earth element.[4] Due to the corresponding difference between the CF strengths, magnetic properties of the pyrochlore terbium and erbium stannates differ qualitatively from properties of the corresponding titanates with relatively small energies of the first excited CF state.[21] The knowledge of the lowest fragment of the energy pattern of magnetic ions is of most importance to interpret the low-

temperature spin-lattice relaxation rates as well.

So far, a limited number of CF energies in a few pyrochlore compounds [$Tm_2Ti_2O_7$,[22] $Er_2Ti_2O_7$,[19] $Tb_2Ti_2O_7$,[8,18,23,24] $Ho_2Ti_2O_7$ (Ref. 25)] were found directly from inelastic neutron scattering experiments. Zero-phonon electric-dipole transitions between energy levels of R^{3+} ions in the CF of D_{3d} symmetry are strictly forbidden. To the best of our knowledge, optical spectra of pyrochlore R oxides have not been studied except the emission, excitation and diffuse reflection spectra in the spectral region of the magnetic dipole $^7F_{J^-}{}^5D_{J'}$ $(J,J'=0,1)$ transitions of Eu^{3+} ions in $Gd_2Ti_2O_7$ and $Eu_2Ti_2O_7$ (see Ref. 26, and references therein), and absorption and luminescence spectra of Nd^{3+} ions in $Y_2Ti_2O_7$ and $Gd_2Ti_2O_7$.[27]

In the present paper, the CF in the $Yb_2Ti_2O_7$ crystals is studied by means of optical spectroscopy. The main goal of this work is to construct the CF Hamiltonian defined by the physically meaningful parameters for R^{3+} ions in pyrochlore oxides and to provide a basis for calculations of single-ion magnetic properties and relaxation rates in different $R_2A_2O_7$ compounds.

Earlier, the temperature dependences of the magnetic susceptibility[5,6,28] and the heat capacity[5] of powdered $Yb_2Ti_2O_7$ samples were studied. The singularity in the heat capacity around 0.21 K was interpreted as a magnetic ordering transition.[5] The Mössbauer spectra were measured in Ref. 29. However, it was not possible to find unambiguously the magnetic spectroscopic g factors of the Yb^{3+} ground state from these measurements. An attempt to find six independent parameters of the CF Hamiltonian for the D_{3d} symmetry by fitting the calculated hyperfine quadrupole parameter, heat capacity and susceptibility to the measured data, and based on the assumption of the easy-axis magnetic anisotropy $(g_\perp=0)$, gave results[30] which appeared inconsistent with the theoretical modeling of the CF and with the experimental data obtained later.[25,31]

Recently, low-temperature magnetic properties of the $Yb_2Ti_2O_7$ crystal have been re-investigated.[31–34] From the ^{170}Yb Mössbauer absorption measurements on the diluted $(Y_{0.99}Yb_{0.01})_2Ti_2O_7$ sample, parameters of the magnetic hyperfine interaction were found and the planar anisotropy of the magnetic moment in the ground state of Yb^{3+} was established. The obtained values of g factors were confirmed by the analysis of the thermal dependence of the susceptibility and the field dependence of the magnetization in the polycrystalline and single crystal $Yb_2Ti_2O_7$ at temperatures 2.5–20 K.[31] The easy-plane anisotropy in $Yb_2Ti_2O_7$ was predicted also earlier in Refs. 25 and 35 from calculations with the CF parameters fitted to the measured CF energies and the temperature dependence of the magnetic susceptibility in $Ho_2Ti_2O_7$. A set of CF parameters presented in Ref. 31 describes satisfactory components of the g tensor of the Yb^{3+} ground Kramers doublet and the temperature dependence of the electric field gradient in $Yb_2Ti_2O_7$ obtained from ^{172}Yb perturbed angular correlation measurements. However, some parameters in this and previous studies[35] differ essentially more than it could be expected from the changes of the lattice structure for different $R_2Ti_2O_7$ crystals, and thus, the question about their reliability and physical meaning remains open.

The paper is organized as follows. After a brief description of experimental details (Sec. II), in Sec. III we present and analyze data of optical measurements on $Yb_2Ti_2O_7$ and $Y_2Ti_2O_7:Yb^{3+}$. In Sec. IV, we calculate the initial values of CF parameters in the framework of the exchange charge model[36] and fit CF parameters to obtain crystal-field energies, g factors, and electric field gradient at the Yb^{3+} nucleus in $Yb_2Ti_2O_7$ in agreement with experimental data. In Sec. V, variation of the CF parameters across the rare-earth series in pyrochlore oxides is discussed.

II. EXPERIMENT

Single crystals of $Yb_2Ti_2O_7$ were grown by the floating-zone technique. The crystals were big, transparent, and of good optical quality. Three samples of different thickness $d_1=1.55$ mm, $d_2=0.60$ mm, and $d_3=90$ μm were prepared for absorption measurements. Absorption spectra in a broad range of frequencies (9000–14 000 cm^{-1}) and temperatures (4.5–300 K) were measured with a Fourier-transform spectrometer BOMEM DA3.002 equipped with a helium-vapor cryostat, at a resolution up to 0.5 cm^{-1}.

$Yb_2Ti_2O_7$ crystals did not luminesce, even at low temperatures, because of a concentration quenching. To measure the emission, diluted polycrystalline samples of $Y_2Ti_2O_7:Yb$ (1 at. %) have been synthesized by solid-state reaction with four intermediate grindings at 1400 °C in air. X-ray analysis confirmed the pyrochlore structure of these synthesized samples and revealed a small amount of residual oxide impurity. A pressed tablet was prepared and attached to a cold finger of a closed-cycle helium cryostat. The temperature of the finger was 10, 80, or 300 K.

The emission spectra under variable wavelength excitation of a cw Ti-sapphire laser (Coherent 890) pumped by an argon ion laser, were recorded with an ARC SpectraPro-7510 monochromator and detected with a cooled InGaAs photodiode. The spectra were not corrected for the spectral sensitivity of the detector. To take the excitation spectra, the intensity at a selected wavelength of the emission was registered as a function of the wavelength of an exciting light.

III. EXPERIMENTAL RESULTS

The $4f^{13}$ configuration of Yb^{3+}, that is a single hole in the $4f$ shell, reveals only two energy levels $^2F_{7/2}$ and $^2F_{5/2}$ separated by about 10 000 cm^{-1}. In a CF of D_{3d} symmetry the ground level $^2F_{7/2}$ splits into four Kramers doublets $3\Gamma_4+\Gamma_{56}$, the excited level $^2F_{5/2}$ splits into three Kramers doublets $2\Gamma_4+\Gamma_{56}$. All the states have the same parity in the D_{3d} symmetry group that contains the center of inversion, therefore, only magnetic-dipole zero-phonon transitions are allowed between them. At low temperature, one should expect a very simple absorption (emission) spectrum consisting of three (four) lines. However, as the electronic-vibrational (vibronic) transitions that involve odd-parity relative displacements of the Yb^{3+} ion and surrounding ions are allowed in the electric-dipole approximation, they may have a comparable or even greater intensity in the case of a sufficiently

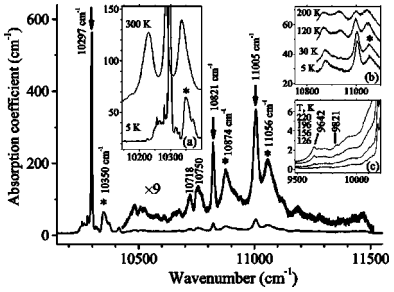

FIG. 1. Absorption spectrum of $Yb_2Ti_2O_7$ at 5 K. Arrows indicate zero-phonon lines, asterisks mark their stokes satellites 52 cm^{-1}. Insets: specific spectral regions at different temperatures.

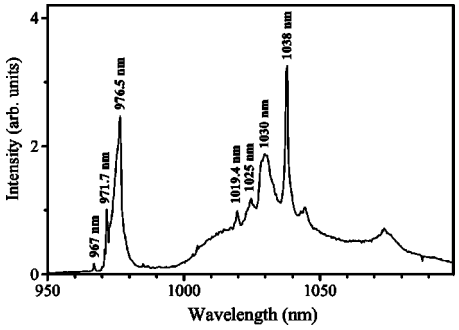

FIG. 2. Luminescence spectrum of $Y_2Ti_2O_7$:Yb(1%) at about 20 K. Wavelength of the excitation λ_{exc}=920 nm.

strong electron-phonon coupling. Just such a case is realized for $Yb_2Ti_2O_7$.

Figure 1 shows the absorption spectrum of $Yb_2Ti_2O_7$. It consists of several relatively narrow lines superimposed onto a broad structured continuum. The latter comes from vibronic transitions and is connected with spectral densities for dynamic lattice deformations corresponding to A_{2u} and E_u irreducible representations of the D_{3d} point group. We note, that lattice vibrations with zero wave vector manifest themselves in the infrared absorption [the infrared absorption peaks of $Yb_2Ti_2O_7$ have been found at 75, 136, 235, 270, 400, 450, and 570 cm^{-1} (Ref. 37)] and in the Raman scattering spectra [the observed Raman-active phonons have the frequencies 220, 320, 525, 590 cm^{-1} (Ref. 37)]. The most intense and narrow line 10 297 cm^{-1} in the absorption spectrum of $Yb_2Ti_2O_7$ has both high- and low-frequency satellites ±52 cm^{-1} at ambient temperature [see Fig. 1, inset (a)]. The low-frequency anti-Stokes satellite disappears on decreasing the temperature, while the high-frequency one develops a clearly resolved shoulder at 75 cm^{-1} from the main line. Possibly, this satellite is connected with the lowest-frequency optical phonon branch, so that the peaks at 52 and 75 cm^{-1} come from vibronic transitions with a participation of the zone-boundary and the zone-center phonons, respectively. We ascribe the mentioned absorption line 10 297 cm^{-1} and the lines 10 821 and 11 005 cm^{-1} to zero-phonon transitions from the ground state to the crystal field levels of $^2F_{5/2}$. The reasons for such an assignment are as follows. (i) These three lines are the most narrow and narrow most strongly on decreasing the temperature. (ii) All three of them are accompanied by vibronic satellites shifted by ±52 cm^{-1} (Stokes satellites are marked by asterisks in Fig. 1), and the anti-Stokes satellites disappear at low temperatures [see insets (a) and (b) of Fig. 1]. A disappearance of the anti-Stokes satellite of the line 10 821 cm^{-1} is masked by the presence of the Stokes satellites 421 and 453 cm^{-1} of the line 10 297 cm^{-1} probably connected with the dispersion branches of infrared-active phonons 400 and 450 cm^{-1}, respectively. (iii) The overall width of the absorption spectrum is well reproduced if we add 590 cm^{-1} (which is the total width of the lattice vibrational spectrum[37]) to each of the mentioned lines. The remaining peaks in the spectral region between the lines 10 297 and 10 821 cm^{-1} can be attributed to the Stokes satellites of the line 10 297 cm^{-1}. Several very narrow lines in a close vicinity of the line 10 297 cm^{-1} are, probably, due to extrinsic Yb^{3+} centers. About 4% of extrinsic Eu^{3+} centers have been found in $Eu_2Ti_2O_7$ and explained by a disorder in oxygen sublattices.[26]

Figure 2 demonstrates the luminescence spectrum of $Y_2Ti_2O_7$:Yb^{3+} at about 20 K upon the excitation at 10 870 cm^{-1}. In this spectrum, the emission of Yb^{3+} in the main compound, $Y_2Ti_2O_7$, and in the Y_2O_3 impurity phase are superimposed. To eliminate undesirable Y_2O_3:Yb^{3+} emission, we recorded the excitation spectra for the main emission peaks. Figure 3 shows the excitation spectra of the 1030 and 1038 nm emission lines. The wavelength of the first line coincides with that for the Y_2O_3:Yb^{3+} emission.[38] The peaks at 10 252, 10 516, and 11 035 cm^{-1} in this first spectrum [see Fig. 3(a)] correspond to well known absorption lines of C_2 (10 252 and 11 035 cm^{-1}1) and S_6 (10 516 cm^{-1}) centers of Y_2O_3:Yb^{3+}.[39] The peaks at 10 291 and 10 341 cm^{-1} come from the main phase $Y_2Ti_2O_7$:Yb^{3+}, due to the presence of its emission at the wavelength of registration. These peaks and the peak at 10 241 cm^{-1} are the most strong in the excitation spectrum of the 1038 nm emission shown in Fig. 3(b). A general view of this excitation

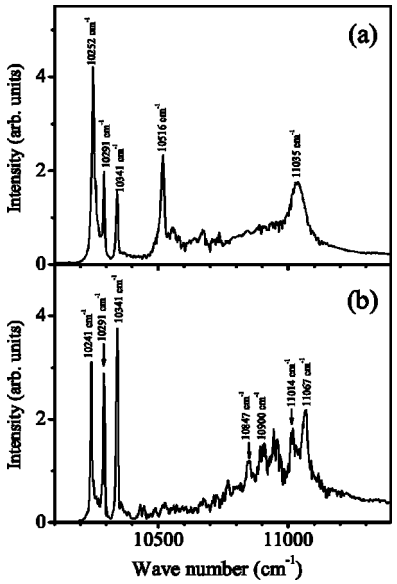

FIG. 3. Excitation spectrum for luminescence of $Y_2Ti_2O_7$:Yb(1%) at λ_{lum}=1030 nm (a) and λ_{lum}=1038 nm (b). $T \cong 20$ K. Arrows indicate zero-phonon absorption lines.

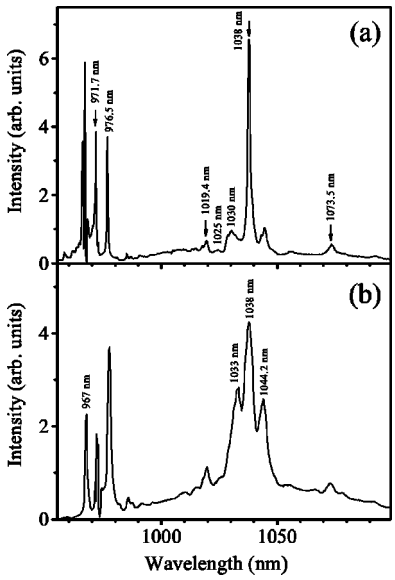

FIG. 4. Luminescence spectra of $Y_2Ti_2O_7$:Yb(1%) under the excitation into the lowest-frequency absorption features [10 341 cm^{-1} (a) or 10 291 cm^{-1} (b)] at $T \cong 20$ K (a) and $T \cong 130$ K (b). Arrows indicate zero-phonon lines.

spectrum very much resembles the absorption spectrum of the concentrated compound $Yb_2Ti_2O_7$. On these grounds, we attribute the emission line 1038 nm to the main center of $Y_2Ti_2O_7:Yb^{3+}$.

The excitation into each of the three lowest-frequency lines (10 241, 10 291, and 10 341 cm^{-1}) results in almost the same luminescence spectrum. It is shown in Fig. 4(a) for the 10 341 cm^{-1} selective excitation. A broad peak at 1030 nm and a weak line at 1025 nm come from the $Y_2O_3:Yb^{3+}$ impurity phase. They grow in intensity for the 10 241 cm^{-1} excitation which is close to the lowest-frequency absorption peak of $Y_2O_3:Yb^{3+}$ at 10 250 cm^{-1}. Figure 4(b) shows the emission of $Y_2Ti_2O_7:Yb^{3+}$ at higher temperature (about 130 K). A comparison of the spectra of Figs. 4(a) and 4(b) leads us to the following assignment of the emission lines in the luminescence spectra of $Y_2Ti_2O_7:Yb^{3+}$. The line 971.7 nm (10 291 nm^{-1}) which is close to the main absorption line 10 297 cm^{-1} of the concentrated compound $Yb_2Ti_2O_7$, corresponds to the transition from the lowest Stark sublevel of the $^2F_{5/2}$ excited level to the lowest ground-state sublevel. It is accompanied by ± 50 cm^{-1} vibronic satellites, the anti-Stokes satellite grows in intensity with increasing the temperature. Similar satellites are observed around the line 1038 nm (9634 cm^{-1}) and, possibly, around the weak lines 1019.4 and 1073.5 nm (9810 and 9315 cm^{-1}). We attribute these lines to the zero-phonon electronic transitions to the excited Stark sublevels of the $^2F_{7/2}$ ground level. This assignment results in the following set for the energies of the ground-state Stark multiplet: 0, 481, 657, 976 cm^{-1}. In the absorption spectrum of a thick sample of the concentrated $Yb_2Ti_2O_7$ crystal at 220 K the peaks are observed at about 476 and 655 cm^{-1} from the main absorption line (10 297 cm^{-1}) at its low-frequency side [see inset (c) of Fig. 1] which is in agreement with the above given assignment. Positions of the electronic levels of Yb^{3+} in $Yb_2Ti_2O_7$ and $Y_2Ti_2O_7:Yb^{3+}$ (1%) found from the absorption, selective emission, and selective excitation spectra are summarized in Table I.

IV. MODEL CALCULATIONS OF CRYSTAL-FIELD ENERGIES AND LINE INTENSITIES

The nearest surrounding of a R^{3+} ion in pyrochlore oxides $R_2Ti_2O_7$ contains two oxygen ions (O1, 8*b* sites) diametrically opposed along the threefold axis, and six others (O2, 48*f* sites) forming a puckered hexagon perpendicular to this axis. The distance $R_1(R-O1)=3^{1/2}a/8$ is determined by the lattice constant a, but the distance $R_2(R-O2)=[(x-0.5)^2+2(1/8)^2]^{1/2}a$ is determined by the additional structural parameter x, which changes in the range 0.326–0.331 through the lanthanide series.[2] Numerical values of distances R_1 and R_2 in Tb, Ho, Y, Er, and Yb compounds are given in Table II. Bond lengths R_1 are essentially less than R_2. As a consequence, O1 and O2 ligands are nonequivalent and we can expect very strong interaction of electrons localized at the 4*f* shell of a R^{3+} ion with the nearest axial ligands (O1). Due to a strong crystal field, the *J*-mixing effect has to be taken into account in the calculations of CF energies and large corrections to results obtained in the framework of a static approximation may be expected due to the electron-phonon interaction.

The effective parametric Hamiltonian acting within the space of 4*f* orbitals of a R^{3+} ion in the crystal field of the D_{3d} symmetry has a general form

$$H_{\mathrm{CF}} = B_0^2 C_0^{(2)} + B_0^4 C_0^{(4)} + B_0^6 C_0^{(6)} + B_3^4 (C_3^{(4)} - C_{-3}^{(4)}) + B_3^6 (C_3^{(6)} - C_{-3}^{(6)}) + B_6^6 (C_6^{(6)} + C_{-6}^{(6)}), \quad (1)$$

where B_q^k are the CF parameters, and $C_q^{(k)}$ are the tensor spherical operators. The CF states correspond to eigenfunctions of the Hamiltonian that includes both free-ion terms and H_{CF} and can be classified according to irreducible representations of the D_{3d} group. The energy pattern of a non-Kramers ion involves singlets A_1 and A_2 and doublet *E* states with magnetic moments along the symmetry axis ($g_\parallel \neq 0$, $g_\perp = 0$). CF states of a Kramers ion are $\Gamma_4(g_\parallel \neq 0,\ g_\perp \neq 0)$ and $\Gamma_{56}(g_\parallel \neq 0,\ g_\perp = 0)$ doublets.

Our goal is to find CF parameters that would allow a satisfactory description of the observed spectra. The initial values of the CF parameters can be estimated in the framework of the exchange-charge model (ECM) that takes into account energies of the valent 4*f* electrons in the electrostatic field of point charges (*PC*) of lattice ions and in the field of exchange charges (*EC*) defined through the overlap integrals between the 4*f* wave functions of the *R* ion and its nearest neighbors.[36] The corresponding terms in the sum

$$B_q^k = B_q^{(PC)k} + B_q^{(EC)k}. \quad (2)$$

are defined by the following formulas:

$$B_q^{(PC)k} = -\sum_L e^2 q_L (1-\sigma_k) \langle 4f|r^k|4f\rangle \beta_k(R_L)(-1)^q \times C_{-q}^{(k)}(\vartheta_L, \varphi_L)/R_L^{k+1}, \quad (3)$$

TABLE I. Energies (cm^{-1}), symmetry (irreducible representation of the D_{3d} group), and magnetic spectroscopic factors of crystal-field sublevels in multiplets of rare-earth ions in $R_2Ti_2O_7$

$Y_2Ti_2O_7$:Yb(1%) experiment		$Yb_2Ti_2O_7(^2F_{7/2},{}^2F_{7/2})$ experim.	calculated		$Er_2Ti_2O_7(^4I_{15/2})$ experim. (Ref. 19)	calculated		$Ho_2Ti_2O_7(^5I_8)$ experim. (Refs. 6,25,35)		calculated		$Tb_2Ti_2O_7(^7F_6)$ experiment (Refs. 17,23)		calculated	
$^2F_{7/2}$	0	0	0	(Γ_4)	0	0	(Γ_4)	0	(E)	0	(E)	0	(E)	0	(E)
	$g_\parallel=1.79$; $g_\perp=4.27$[a]		$g_\parallel=1.836$; $g_\perp=4.282$		$g_\perp>6$	$g_\parallel=2.32$; $g_\perp=6.8$		$g_\parallel=18.70$		$g_\parallel=19.32$		$g_\parallel=10.2\pm0.6$		$g_\parallel=10.4$	
	481	476	528	(Γ_4)	51	51.6	(Γ_{56})			166	(A_2)	12.1 ± 0.5	(E)	12.1	(E)
												$g_\parallel=11.8\pm1.6$		$g_\parallel=13.4$	
	657	655	649	(Γ_{56})	59	58.8	(Γ_4)	177.4	(E)	177	(E)	83.5 ± 0.7		76.4	(A_2)
	976		972	(Γ_4)		135	(Γ_4)	209.7	(E)	213	(E)	116.7		120	(A_1)
$^2F_{5/2}$	10 291	10 297	10 293	(Γ_4)		447	(Γ_4)			224	(A_1)			284	(E)
	10 847	10 821	10 736	(Γ_4)		458	(Γ_{56})	475.8	(E)	471	(E)			314	(A_2)
	11 014	11 005	11 004	(Γ_{56})		490	(Γ_4)			545	(A_1)			318	(A_1)
						710	(Γ_{56})			564	(A_2)			439	(E)
								572.6	(E)	565	(E)			510	(A_1)
								621	(E)	617	(E)				
										647	(A_1)				

[a]Ref. 31.

$$B_q^{(EC)k}=\sum_L \frac{2(2k+1)}{7}\frac{e^2}{R_L}S_k(R_L)(-1)^q C_{-q}^{(k)}(\vartheta_L,\varphi_L). \quad (4)$$

Here eq_L is the net charge of the lattice ion L with the spherical coordinates R_L,θ_L,φ_L (the origin of the coordinates is at the R ion), σ_k are the shielding factors,[40] $-e\langle 4f|r^k|4f\rangle$are the moments of the $4f$ electron charge distribution,[41] and $\beta_k(R_L)$ are the correction factors in the Coulombic energy of the extended charge distributions of the R and ligand ions.[42] If ligand ions have filled ns^2 and np^6 electron shells, only the outer shells ($n=2$ for oxygen ions) with the largest overlap integrals

$$S_s^n(R_L)=\langle 4f0|ns\rangle,\quad S_\sigma^n(R_L)=\langle 4f0|np0\rangle,\quad S_\pi^n(R_L)=\langle 4f1|np1\rangle \quad (5)$$

can be considered, and exchange charge contributions are defined by phenomenological parameters G_s,G_σ,G_π in the linear combinations of the squared overlap integrals

TABLE II. Bond lengths (nm) between the rare-earth and the nearest-neighbor oxygen ions [$R(R-O1)=R_1,R(R-O2)=R_2$] (Refs. 2,3) and crystal field parameters $B_p^{\ k}$ (cm^{-1}) in rare-earth titanate pyrochlores.

	$Tb_2Ti_2O_7$	$Ho_2Ti_2O_7$			$Er_2Ti_2O_7$	$Tm_2Ti_2O_7$	$Yb_2Ti_2O_7$	$Y_2Ti_2O_7:Yb^{3+}$	
R_1	0.2194	0.2187			0.2182	0.2179	0.2172	0.2187	
R_2	0.2496	0.2489			0.2488	0.2474	0.2454	0.2477	
1	2	3	4		5	6	7	8	
	[a]	(Ref. 35)	[a]	[b]	[a]	[a]	(Ref. 31)	[a]	[b]
B_0^2	440	550 ± 18	532	(552)	534	540	539	546	(590)
B_0^4	2535	2216 ± 14	2475	(2476)	2524	2510	569	2540	(2186)
B_0^6	850	701 ± 7	805	(782)	748	850	1568	840	(822)
B_3^4	735	675 ± 9	716	(700)	698	670	916	602	(611)
B_3^6	−630	-504 ± 5	−596	(−583)	−521	−505	−510	−462	(−498)
B_6^6	850	819 ± 9	838	(845)	755	755	790	757	(701)

[a]Results of fitting the calculated spectra to the experimental data.
[b]Parameters obtained in the framework of ECM.

$$S_k(R_L) = G_s[S_s^n(R_L)]^2 + G_\sigma[S_\sigma^n(R_L)]^2 + [2 - k(k+1)/12]G_\pi[S_\pi^n(R_L)]^2. \quad (6)$$

In the definitions of the overlap integrals (5), wave functions of the R^{3+} ($|4fl_z\rangle$) and ligand ($|nlll_z\rangle$) ions are considered in the reference systems with the common quantization z axis. Numerical values of the overlap integrals used in this work were calculated with the radial functions from Refs. 41 ($4f$ functions of R^{3+} ions) and[43] (O^{2-}).

To find the values of model parameters G_s, G_σ, G_π we used the following procedure. First, we considered the case of $Ho_2Ti_2O_7$, where the most reliable set of CF parameters in pyrochlore oxides was obtained.[35] These parameters are given in column 3 of Table II. However, in Ref. 35, the CF energies were calculated with the Hamiltonian (1) defined in the limited space of the ground multiplet ($^5I_8$) states. Taking into account the spin-orbit, electrostatic and crystal-field interactions within the total space of states of the $4f^{10}$ configuration, we obtained the set of CF parameters (column 4a in Table II) which are slightly different from those given in Ref. 35. The calculated with these parameters and measured CF energies and g factor of the Ho^{3+} ground doublet are compared in Table I. As the next step in the analysis of the crystal field in pyrochlore oxides, we determined parameters of the ECM for $Ho_2Ti_2O_7$ corresponding to the fitted CF parameters. The Coulombic contributions to the CF parameters (3) were calculated using point ion charges $-2e$ (oxygen), $+4e$ (Ti), and $+3e$ (R). As the interaction of a R^{3+} ion with O1 ligand ions does not contribute to parameters B_p^k with $p \neq 0$, it is easy to find, using the simplest relations between the parameters G_α,[36,44] the independent values $G_\sigma = G_s = G_\pi = 9.65$ for O1 ligands and $G_\sigma = G_s = G_\pi/0.8 = 16.55$ for O2 ligands that allow to obtain the corresponding six CF parameters (column 4b of Table II), in good agreement with the experimental data. Further, we used thus determined relations between the model parameters for Ho^{3+} in the pyrochlore titanate $Ho_2Ti_2O_7$ and the values of these parameters for Yb^{3+} surrounded by oxygen atoms in the $Yb_3Al_5O_{12}$ garnet[45] to get the following values of model parameters for Yb^{3+} in $Yb_2Ti_2O_7$: $G_\sigma = G_s = G_\pi = 13.5$; $G_\sigma = G_s = G_\pi/0.8 = 20$ for O1 and O2 ligand ions, respectively.

They were used at the next step to calculate the initial values of CF parameters in $Yb_2Ti_2O_7$ (see column 8b in Table II). At last, starting from this set, we varied the CF parameters to obtain the CF energies and wave functions consistent with the measured frequencies of optical zero-phonon transitions, components of the g tensor in the ground state and relative thermal variation of the canonical average of the electronic quadrupole moment that determines the electric-field gradient (EFG) at the Yb^{3+} nucleus[31]

$$V_{zz}(T) = V_{zz}(\infty) + [V_{zz}(0) - V_{zz}(\infty)]\frac{\langle l_z^2 - 3l(l+1)\rangle_T}{\langle l_z^2 - 3l(l+1)\rangle_0}. \quad (7)$$

The numerical diagonalization of the Hamiltonian

$$H[4f^{13}] = -H_{CF} - \zeta \mathbf{l}\cdot\mathbf{s}. \quad (8)$$

($\zeta = 2892$ cm^{-1} is the constant of the spin-orbit coupling, $\mathbf{l}$ and $\mathbf{s}$ are the orbital and spin moments, respectively) was performed in the space of 14 spin orbitals of a hole in the $4f$ shell. The fitted CF parameters are represented in Table II (column 8a). The calculated CF energies, g factors of the ground state and the EFG are compared with the experimental data in Table I and Fig. 5. From this comparison, we see that the greatest discrepancy is found for the position of the second Γ_4 sublevel of the excited CF manifold $^2F_{5/2}$. The calculated energy is underestimated up to 100 cm^{-1}. It is possible to obtain the correct values of g factors and the energy of this sublevel close to the experimental value by introducing the B_0^2 parameter larger than 650 cm^{-1}. However, in this case the energy of the first excited sublevel in the ground manifold $^2F_{7/2}$ also increases, and the corresponding temperature dependence of the EFG disagree with the experimental data. Again, with the B_0^2 parameter lower and the B_0^6 parameter higher by about 100 cm^{-1} than the corresponding values of these parameters given in column 8a of Table II, it is possible to describe satisfactorily all experimental findings except the position of the same Γ_4 sublevel of the excited CF manifold $^2F_{5/2}$.

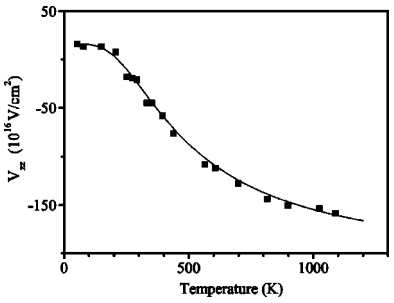

FIG. 5. Temperature dependence of the electric-field gradient at the ^{172}Yb nucleus measured by the perturbed angular correlations technique (symbols) (Ref. 31) and calculated in the present work (solid line).

It has been shown earlier by one of the authors that the plot of the center of gravity of the $^2F_{5/2}$ CF manifold vs the center of gravity of the $^2F_{7/2}$ ground-state manifold for different known Yb compounds can be well approximated by a straight line, the so called barycenter curve.[46,47] We used this curve to check our data on CF levels of Yb^{3+} in $Y_2Ti_2O_7$. Both the experimental set of energy levels and the calculated one reveal the points situated close to the mentioned barycenter curve (see Fig. 6). On the contrary, the CF energies (0, 452, 530, 672, 10 291, 10 565, 10 716) calculated using the set of CF parameters suggested in Ref. 31 give the position of the center of gravity for $^2F_{7/2}$ at 414 cm^{-1} and, according with the barycenter curve, the value of 10 524 cm^{-1} for the center of gravity of $^2F_{5/2}$, which is inconsistent with the absorption spectrum of $Yb_2Ti_2O_7$ presented in this work.

The interpretation of the absorption and emission spectra of $Yb_2Ti_2O_7$ and $Y_2Ti_2O_7$:Yb presented above is consistent with intensities of magnetic dipole transitions between the CF energy levels of Yb^{3+} ions expected from calculations. Matrix elements of the magnetic dipole moment were calculated in the basis of eigenfunctions $|\Gamma\sigma\rangle$ of the Hamiltonian (8) determined by the CF parameters from column 8a of Table II, and the relative transition probabilities

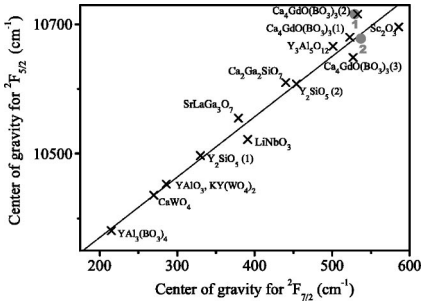

FIG. 6. Center of gravity of the $^2F_{5/2}$ CF manifold vs the center of gravity of the $^2F_{7/2}$ ground manifold plotted for Yb^{3+} ions in different compounds (crosses). The numbers in brackets after chemical symbols refer to different Yb^{3+} positions in a compound. Circles correspond to the experimental (1) and calculated (2) data for $Yb_2Ti_2O_7$. The straight line is a guide for the eye.

$$W_{\Gamma\to\Gamma'} \sim \sum_{\sigma\sigma'} \sum_{\alpha=x,y,z} |\langle \Gamma\sigma | l_\alpha + 2s_\alpha | \Gamma'\sigma' \rangle|^2 \qquad (9)$$

are given in Table III. The relative integrated intensities of the optical zero-phonon transitions found from the absorption spectra (1.0:0.09:0.22) are in reasonable agreement with the calculated ones (see column 1 in Table III). The luminescence spectra did not allow one to perform quantitative measurements because of reabsorption of the resonance line 10 291 cm^{-1}. However, the observed intensities are in a qualitative agreement with the calculated ones, the third zero-phonon line being the strongest one (see Figs. 2 and 4 and row 1 in Table III).

V. DISCUSSION

In the previous section, we have obtained the set of CF parameters for $Yb_2Ti_2O_7$ that satisfactory describes the line position (except the position of the second Γ_4 sublevel of the $^2F_{5/2}$ level) and intensities in the optical spectra observed in this work, as well as magnetic g factors[31] and the temperature dependence of the electric-field gradient at the Yb^{3+} nucleus.[31] The impossibility to reproduce the whole energy spectrum of the $4f^{13}$ configuration of Yb^{3+} in the pyrochlore titanate well may be connected with energy shifts by a relatively strong electron-phonon interaction not taken into account in the present work. On the other hand, it should be noted that lattice disorder effects may influence the observed spectra,[26,27] and the possibility of misinterpretation of spectral lines cannot be entirely excluded. We can additionally check the obtained results by studying trends in a variation of the CF parameters along the series of R compounds with pyrochlore structure. The available information about different compounds is rather limited and involves mainly data on magnetic spectroscopic factors in the ground state and the energy of the first excited CF sublevel of a R^{3+} ion. However, it is important to know whether the CF parameters obtained in this study are consistent with these data and can be used to predict magnetic and spectral properties of other R pyrochlore oxides.

Starting from the CF parameters for $Yb_2Ti_2O_7$, we obtained the sets of parameters for $Tb_2Ti_2O_7$, $Er_2Ti_2O_7$, and $Tm_2Ti_2O_7$ presented in columns 2, 5, and 6 of Table II. Using these CF parameters, we simulated CF energies and g-tensor components. They agree well with the experimental data. Table I presents the comparison between the experimental and calculated values for $Tb_2Ti_2O_7$ and $Er_2Ti_2O_7$. Tm^{3+} ions in $Tm_2Ti_2O_7$ have the singlet ground state, and the energy of the first excited doublet is 85 cm^{-1}, according to results of inelastic neutron scattering and dc-susceptibility measurements.[22] The calculated energy of the first excited doublet equals 79 cm^{-1}, and other sublevels have energies higher than 250 cm^{-1}. From the simulation of CF energies and wave functions of the Dy^{3+} ion with the CF parameters of the $Tb_2Ti_2O_7$ crystal, we obtain the ground doublet Γ_{56}, well isolated from the excited CF states at energies higher than 200 cm^{-1}, with the $g_\parallel$ factor equal to 19.2 in agreement with the g factor of 18.5 measured for $Dy_2Ti_2O_7$.[6]

The sets of CF parameters for the pyrochlore titanates $R_2Ti_2O_7$ obtained in this work for the series of R ions with the increasing number of $4f$ electrons possess the following remarkable feature. While the absolute values of the parameters B_3^4, B_3^6, and B_6^6 that are determined, mainly, by the interaction between $4f$ electrons and distant O2 ligands, decrease along the series (which is usually observed for different structures), the parameters B_0^2, B_0^4, and B_0^6 that have the dominant contribution from the nearest ligands O1, remain almost constant (see rows a in Table II). Such a behavior of CF parameters is consistent with the trends in variations of the ratios of angular overlap model parameters (bond energies) to the corresponding squared overlap integrals with changes of the bond lengths.[44]

In conclusion, it is worth mentioning that we can expect similar values of the CF parameters in R titanates, stannates, molibdates, and niobates with the pyrochlore structure, and the results of the present work can be used to analyze measured magnetic properties of R stannates,[21] $Yb_2Mo_2O_7$,[48] and $Tb_2Nb_2O_7$.[49]

VI. SUMMARY

We have measured temperature-dependent absorption spectra of $Yb_2Ti_2O_7$ single crystals and emission and excita-

TABLE III. Calculated relative intensities of magnetic dipole transitions between CF sublevels of $^2F_{7/2}$ and $^2F_{5/2}$ multiplets of Yb^{3+} ions in $Yb_2Ti_2O_7$.

$\Gamma(^2F_{5/2})\backslash\Gamma'(^2F_{7/2})$	1 (0 cm^{-1})	2 (478 cm^{-1})	3 (657 cm^{-1})	4 (977 cm^{-1})
1 (10297 cm^{-1})	1.000	0.193	1.338	0.093
2 (10821 cm^{-1})	0.171	1.596	0.241	0.790
3 (11005 cm^{-1})	0.298	0.124	0.928	1.822

tion spectra of $Y_2Ti_2O_7:Yb^{3+}$ (1%) polycrystalline samples. The energies of all the crystal-field levels within the $4f^{13}$ configuration of Yb^{3+} in titanates with the pyrochlore structure have been found from the analysis of the spectra. We have performed the crystal-field calculations, starting from the model calculations in the framework of the exchange-charge model, and obtained the set of CF parameters that describes satisfactory the optical spectra observed in this work as well as experimental data obtained earlier on magnetic *g* factors and the temperature dependence of the electric-field gradient at the Yb^{3+} nucleus. Starting from the CF parameters for $Yb_2Ti_2O_7$, we obtained the sets of CF parameters for different other $R_2Ti_2O_7$ compounds and used them to calculate CF energies and *g* factors. A comparison between the calculated and experimental values (known from earlier works) always revealed good agreement. This gave us a possibility to analyze the trends in the variation of CF parameters along the series of *R* titanates with pyrochlore structure. Unusual stability of the B_0^2, B_0^4, and B_0^6 parameters has been explained by considering the role of nonequivalent O1 and O2 oxygen ligands. The results of this work can be used to analyze and predict magnetic and spectral properties of other *R* oxides with the pyrochlore structure.

ACKNOWLEDGMENTS

This work was partly supported by the Russian Foundation for Basic Research under Grants Nos. 03-02-16449 and 04-02-17346 and by the RAS-CNRS cooperation program (Project No. 12234).

[1] O. Knop, F. Brisse, and L. Castelliz, C. R. Seances Acad. Sci., Ser. D **47**, 971 (1969).
[2] J. Lian, J. Chen, L.M. Wang, R.C. Ewing, J.M. Farmer, L.A. Boatner, and K.B. Helean, Phys. Rev. B **68**, 134107 (2003).
[3] S.-W. Han, J.S. Gardner, and C.H. Booth, Phys. Rev. B **69**, 024416 (2004).
[4] B.J. Kennedy, B.A. Hunter, and C.J. Howard, J. Solid State Chem. **130**, 58 (1997).
[5] H.W.J. Blöte, R.F. Wielinga, and H. Huiskamp, Physica (Amsterdam) **43**, 549 (1969).
[6] S.T. Bramwell, M.N. Field, M.J. Harris, and I.P. Parkin, J. Phys.: Condens. Matter **12**, 483 (2000).
[7] A.P. Ramirez, *Handbook on Magnetic Materials* (Elsevier, Amsterdam, 2001), Vol. 13, Chap. 4, p. 423.
[8] J.S. Gardner, S.R. Dunsiger, B.D. Gaulin, M.J.P. Gingras, J.E. Greedan, R.F. Kiefl, M.D. Lumsden, W.A. MacFarlane, N.P. Raju, J.E. Sonier, I. Swainson, and Z. Tun, Phys. Rev. Lett. **82**, 1012 (1999).
[9] J.S. Gardner, A. Keren, G. Ehlers, C. Stock, Eva Segal, J.M. Roper, B. Fak, M.B. Stone, P.R. Hammar, D.H. Reich, and B.D. Gaulin, Phys. Rev. B **68**, 180401 (2003).
[10] S.R. Dunsiger, R.F. Kiefl, J.A. Chakhalian, K.H. Chow, J.S. Gardner, J.E. Greedan, W.A. MacFarlane, R.I. Miller, G.D. Morris, A.N. Price, N.P. Raju, and J.E. Sonier, Physica B **326**, 475 (2003).
[11] Gang Luo, S.T. Hess, and L.R. Corruccini, Phys. Lett. A **291**, 306 (2001).
[12] M.J. Harris, S.T. Bramwell, D.F. McMorrow, T. Zeiske, and K.W. Godfrey, Phys. Rev. Lett. **79**, 2554 (1997).
[13] M.J. Harris, S.T. Bramwell, T. Zeiske, D.F. McMorrow, and P.J.C. King, J. Magn. Magn. Mater. **177–181**, 757 (1998).
[14] H. Fukazawa, R.G. Melko, R. Higashinaka, Y. Maeno, and M.J.P. Gingras, Phys. Rev. B **65**, 054410 (2002).
[15] B.C. den Hertog, M.J.P. Gingras, S.T. Bramwell, and M.J. Harris, cond-mat/9912220 (unpublished).
[16] S.T. Bramwell, M.J. Harris, B.C. den Hertog, M.J.P. Gingras, J.S. Gardner, D.F. McMorrow, A.R. Wildes, A.LO. Cornelius, J.D.M. Champion, R.G. Melko, and T. Fennell, Phys. Rev. Lett. **87**, 047205 (2001).
[17] A.P. Ramirez, A. Hayashi, R.J. Cava, R. Siddharthan, and B.S. Shastry, Nature (London) **399**, 333 (1999).
[18] M.J.P. Gingras, B.C. den Hertog, M. Faucher, J.S. Gardner, S.R. Dunsiger, L.J. Chang, B.D. Gaulin, N.P. Raju, and J.E. Greedan, Phys. Rev. B **62**, 6496 (2000).
[19] J.D.M. Champion, M.J. Harris, P.C.W. Holdsworth, A.S. Wills, G. Balakrishnan, S.T. Bramwell, E. Cizmar, T. Fennell, J.S. Gardner, J. Lago, D.F. McMorrow, M. Orendac, A. Orendacova, D.McK. Paul, R.I. Smith, M.T.F. Telling, and A. Wildes, Phys. Rev. B **68**, 020401 (2003).
[20] R.G. Melko, B.C. den Hartog, and M.J.P. Gingras, Phys. Rev. Lett. **87**, 067203 (2001).
[21] K. Matsuhira, Y. Hinatsu, K. Tenya, H. Amitsuka, and T. Sakakibara, J. Phys. Soc. Jpn. **71**, 1576 (2002).
[22] M.P. Zinkin, M.J. Harris, Z. Tun, R.A. Cowley, and B.M. Wanklyn, J. Phys.: Condens. Matter **8**, 193 (1996).
[23] J.S. Gardner, B.D. Gaulin, A.J. Berlinsky, P. Waldron, S.R. Dunsiger, N.P. Raju, and J.E. Greedan, Phys. Rev. B **64**, 224416 (2001).
[24] Y-J. Kao, M. Enjalran, and M.J.P. Gingras, cond-mat/0207270 (unpublished).
[25] R. Siddharthan, B.S. Shastry, A.P. Ramirez, A. Hayashi, R.J. Cava, and S. Rosenkranz, Phys. Rev. Lett. **83**, 1854 (1999).
[26] P.A.M. Berdowski and G. Blasse, J. Solid State Chem. **62**, 317 (1986).
[27] V.A. Antonov, P.A. Arsenev, and D.S. Petrova, Phys. Status Solidi A **41**, K127 (1977).
[28] M.G. Townsend and W.A. Crossley, J. Phys. Chem. Solids **29**, 593 (1968).
[29] B.D. Dunlap, G.K. Shenoy, J.M. Friedt, M. Meyer, and G.J. McCarthy, Phys. Rev. B **18**, 1936 (1978).
[30] A. Sengupta, J. Jana, and D. Ghosh, J. Phys. Chem. Solids **60**, 331 (1999).
[31] J.A. Hodges, P. Bonville, A. Forget, M. Rams, K. Krolas, and G. Dhalenne, J. Phys.: Condens. Matter **13**, 9301 (2001).
[32] J.A. Hodges, P. Bonville, A. Forget, A. Yaouanc, P. Dalmas de Reotier, G. Andre, M. Rams, K. Krolas, C. Ritter, P.C.M. Gubbens, C.T. Kaiser, P.J.C. King, and C. Baines, Phys. Rev. Lett. **88**, 077204 (2002).
[33] A. Yaouanc, P. Dalmas de Reotier, P. Bonville, J.A. Hodges, P.C.M. Gubbens, C.T. Kaiser, and S. Sakarya, Physica B **326**,

456 (2003).
[34] P. Bonville, J.A. Hodges, E. Bertin, J.-Ph. Bouchaud, M. Ocio, P. Dalmas de Reotier, L.-P. Regnault, H.M. Ronnow, J.P. Sanchez, S. Sosin, A. Yaouanc, M. Rams, and K. Krolas, cond-mat/0306470 (unpublished).
[35] S. Rosenkranz, A.P. Ramirez, A. Hayashi, R.J. Cava, R. Siddharthan, and B.S. Shastry, J. Appl. Phys. **87**, 5914 (2000).
[36] B.Z. Malkin, in *Spectroscopy of Solids Containing Rare Earth Ions*, edited by A.A. Kaplyanskii and R.M. Macfarlane (North-Holland, Amsterdam, 1987), Chap. 2, p. 13.
[37] M.T. Vandenborre, E. Husson, J.P. Chatry, and D. Michel, J. Raman Spectrosc. **14**, 63 (1983).
[38] E. Mix, Ph.D. thesis, Hamburg University, Aachen 1999.
[39] E. Antic-Fidancev, J. Holsa, and M. Lastusaari, J. Phys.: Condens. Matter **15**, 863 (2003).
[40] R.P. Gupta and S.K. Sen, Phys. Rev. A **7**, 850 (1973).
[41] A.J. Freeman and R.E. Watson, Phys. Rev. **127**, 2058 (1962).
[42] D. Garcia and M. Faucher, Phys. Rev. B **30**, 1703 (1984).
[43] E. Clementi and A.D. McLean, Phys. Rev. **133**, 419 (1964).
[44] M. Faucher, D. Garcia, and C.K. Jørgensen, Chem. Phys. Lett. **129**, 387 (1986).
[45] G.A. Bogomolova, L.A. Bumagina, A.A. Kaminskii, and B.Z. Malkin, Sov. Phys. Solid State **19**, 1428 (1977).
[46] E. Antic-Fidancev, J. Alloys Compd. **300–301**, 2 (2000).
[47] P.-H. Haumesser, R. Gaumé, B. Viana, E. Antic-Fidancev, and D. Vivien, J. Phys.: Condens. Matter **13**, 5427 (2001).
[48] J.A. Hodges, P. Bonville, A. Forget, J.P. Sanchez, P. Vulliet, M. Rams, and K. Krolas, Eur. Phys. J. B **33**, 173 (2003).
[49] Y.M. Jana, O. Sakai, R. Higashinaka, H. Fukazawa, Y. Maeno, P. Dasgupta, and D. Ghosh, Phys. Rev. B **68**, 174413 (2003).